Boosting blister formation on EUV masks by hydrogen and water vapor

Naoki Hayase,[a] Hayato Ishida,[a] Wataru Nishida,[b] Keishi Tsukiyama,[b] Shinji Yamakawa,[a] Tetsuo Harada[a*]

[a] Center for EUV lithography, LASTI, University of Hyogo, 1-1-2 NewSUBARU synchrotron radiation facility, Ako-gun Kouto, Hyogo 678-1205, Japan

[b] AGC Inc. Yokohama Technical Center 1-1, Suehiro-cho, Tsurumi-ku, Yokohama-shi, Kanagawa 230-0045 Japan

Abstract: Blister formation on extreme ultraviolet (EUV) masks by EUV-induced plasma irradiation is a problem that causes patterning errors. We investigated the blister formation under EUV-induced plasma containing hydrogen and water vapor through an accelerated mask lifetime test. **Background:** Interaction between hydrogen gas and EUV radiation generates hydrogen ions and radicals which react with contaminants. Hydrogen gas is introduced in EUV scanners to remove contaminants, but EUV-induced hydrogen plasma forms blisters on EUV masks. Accelerated mask lifetime tests have reported on EUV-induced hydrogen plasma durability but the effect of water vapor on blister formation remains unclear. **Aim:** We evaluate the impact of water vapor on blister formation through EUV accelerated mask lifetime tests at NewSUBARU synchrotron radiation facility. **Approach:** The EUV intensity was in the range of approximately 20 to 47 W/cm², and hydrogen pressure was varied from 5 to 70 Pa with and without water vapor during 10^{-3} to 10^{-1} Pa. The hydrogen pressures were controlled, and the EUV dose was determined from the blister formation time in accelerated mask lifetime tests. The surface oxidation of the irradiated positions on the EUV masks was investigated by X-ray absorption spectroscopy (XAS), Rutherford backscattering spectrometry (RBS), and hydrogen forward scattering spectrometry (HFS). **Results:** The blister formation dose decreased from 500.0 to 229.6 kJ/cm² as the hydrogen pressure increased from 15 to 70 Pa. Adding water vapor at 10^{-3} Pa lowered the dose at every hydrogen pressure and triggered blister formation at 5 Pa. Hydrogen was found to penetrate through the absorber and the Ru capping layer into the Mo/Si multilayer at the irradiated positions. **Conclusion:** We clarify that the water vapor significantly affects the EUV dose and hydrogen pressure thresholds for blister formation. The result provides insight into plasma-induced oxidation and contributes to mask process development.

Keywords: EUV; EUV-induced plasma; hydrogen; water vapor; mask blank; photomask.

E-mail: hayase@lasti.u-hyogo.ac.jp

1 Introduction

Extreme ultraviolet (EUV) lithography has been adopted for high-volume manufacturing at the 7 nm node process and beyond [1]. EUV scanners introduce hydrogen as background gas in order to maintain the cleanliness of the inner walls, mirrors, and photomasks [2-5]. EUV light ionizes and dissociates hydrogen to generate plasma, which causes layer delamination on EUV masks, known as "blister" in Fig. 1 [6-10]. To investigate the blister formation process, EUV accelerated lifetime testing tools with hydrogen gas have been developed to reproduce EUV lithography in a shorter time [11-17]. The relationship between blister formation and EUV-induced hydrogen plasma exposure conditions has been reported [18-22]. Furthermore, it is important to consider how oxygen modifies surface oxidation to reproduce scanner-relevant blistering [23].

EUV irradiation of surfaces leads to photoemission and secondary electron generation [24-26]. In the absence of oxidation, hydrogen produced in the plasma diffuses to interfaces and voids, where it recombines into molecular hydrogen and builds up internal pressure; delamination occurs once this pressure, together with the residual film stress, exceeds the interfacial adhesion energy. Oxidation shifts this balance. In the Cabrera-Mott mechanism, electrons tunnelling from the metal ionize adsorbed oxygen species, and the resulting charge separation establishes a field across the oxide that sustains oxide growth at temperatures where thermal diffusion is negligible [27-30]. Under EUV irradiation, secondary electrons supply these electrons and dissociate adsorbed water, so that a comparable field-driven oxidation may proceed at room temperature. Interfacial oxidation is expected to lower the adhesion energy, so that less accumulated hydrogen is needed to initiate delamination [31-33].

In this paper, we investigated blister formation process on EUV masks exposed to hydrogen and water vapor. Our measurement evaluated the dependences of the pressure and EUV intensity via the accelerated lifetime tests at NewSUBARU synchrotron radiation facility [13].

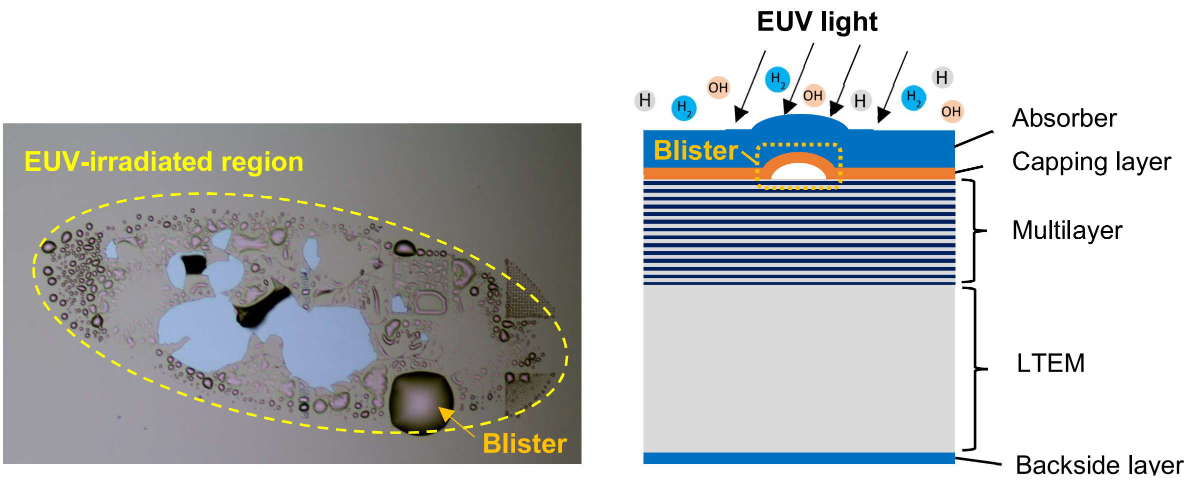

Fig. 1 (a) Image of blister on EUV mask surface (Ref [10]), (b) Schematic of blister on EUV masks.

2 Equipment

2.1 Accelerated mask lifetime test

Fig. 2-(a) shows the beamline 9C (BL9C) at NewSUBARU synchrotron radiation facility. BL9C is served by a 10.8 m undulator with the monochromator at the zeroth diffraction order and the undulator gap at 35 mm, the spectrum is centered at 13.5 nm with a bandwidth of 0.6 nm (FWHM), approximately matching the 0.5 nm reflection bandwidth of the Mo/Si multilayer (ML) [13]. The wavelength is fixed by the gap and ring energy and showed no shift during irradiation. The ring runs in multibunch mode at around 500 MHz, giving 60 pico-second pulses spaced by 2 ns. BL9C provides hydrogen via a water electrolysis generator with a hydrogen purifier, and pure water in Fig. 2-(b) and (c). EUV intensity for the accelerated mask lifetime test is calculated by Eq. (1).

$$\phi_{\mathrm{EUV}} = \frac{I}{S} \times \frac{1}{a \times b} \times \frac{1}{\tau} \tag{1}$$

where I is the beam current of photodiode, S is the measured sensor sensitivity, a and b are width and height of the beam spot, τ is the transmittance of the attenuation filter. In this study, we used a photodiode with S of 0.102 A/W, τ is 1/40. The beam size of a and b are approximately 0.8 mm and 0.3 mm, and we calculate these by the full-width half maximum of image contrast in each test. ϕ_{EUV} exceeds the peak intensity of an equivalent Gaussian profile by about 13 %.

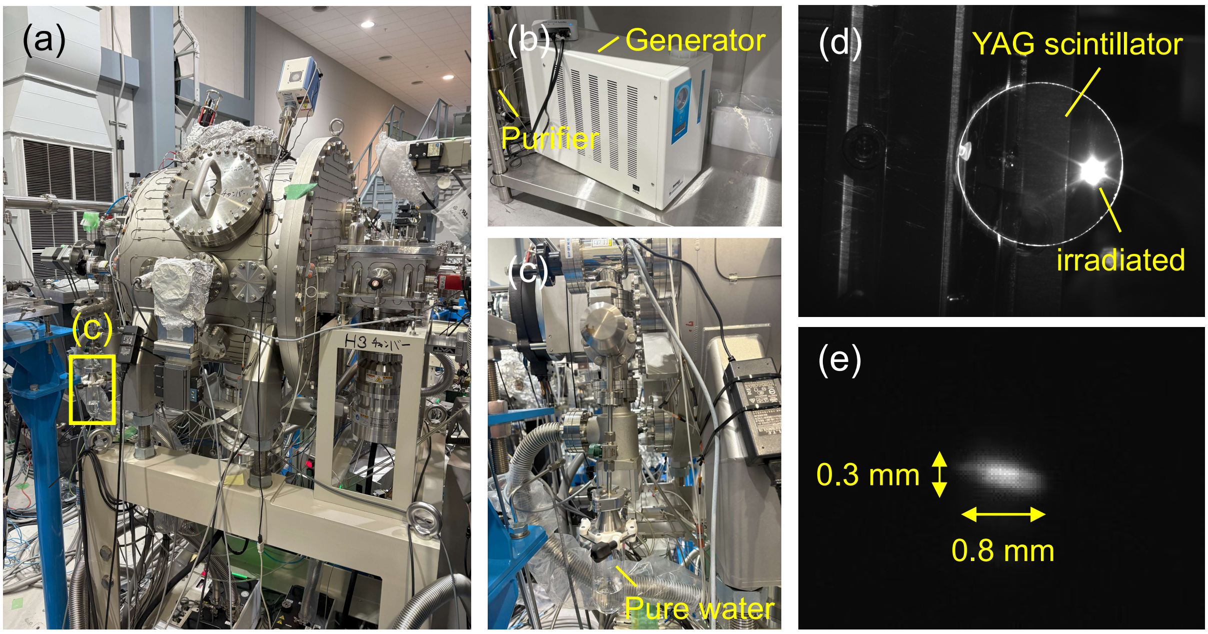

Fig. 2 (a) Overview of BL9C at NewSUBARU synchrotron radiation facility, (b) The electrolysis hydrogen generator with purifier, (c) The pure water supplier, (d) YAG scintillator, (e) The EUV beam spot.

A YAG scintillator and a visible camera were used to image the beam spot size in Figs. 2-(d) and (e), while measuring the beam current by photodiode. The cumulative dose for blister formation can be derived by the integration of the measured intensity by the blister formation time as Eq. (2).

$$Dose = \int_0^{t_{blister}} \phi_{\mathrm{accl}} dt \tag{2}$$

where ϕ_{accl} is the EUV intensity of accelerated exposure test, $t_{blister}$ is the blister formation time. The chamber is evacuated by a turbomolecular pump with two 3 mm orifices for differential pumping toward the beamline. The chamber was not baked, and the base pressure before gas introduction was of the order of 10^{-6} Pa. Hydrogen was admitted through a variable leak valve and measured with a capacitance manometer, whose reading is species-independent and therefore unaffected by the different pumping speeds for hydrogen and heavier gases. Water vapour was supplied through a separate leak valve and its pressure taken from the cold cathode gauge, which is calibrated for nitrogen; this value is thus nominal, with an uncertainty of a few tens of percent. Gases were allowed to stabilize before the shutter was opened, and pressures were held within ±1% during irradiation.

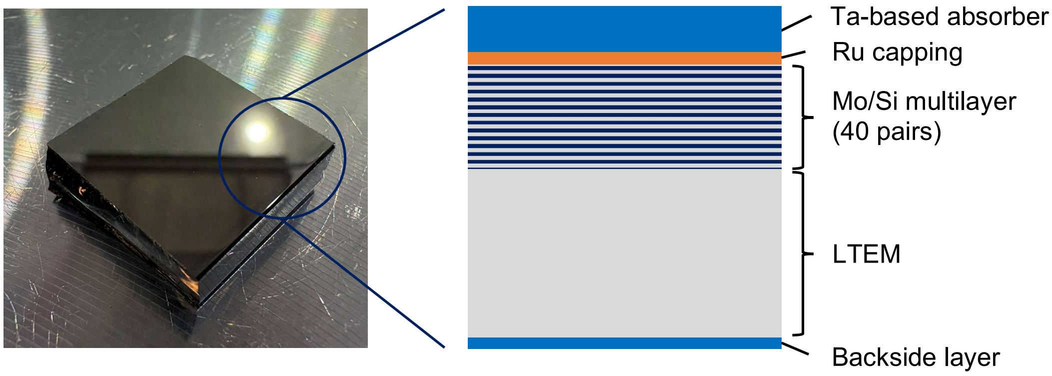

Fig. 3 The image of EUV mask blank fragment (20 mm × 20 mm) and the schematic of EUV mask blank.

2.2 Mask blanks and Photomasks

Fig. 3 shows the EUV mask blank fragments provided by AGC. The mask blanks are configured with Mo/Si ML of 40 pairs, Ru capping layer, and Ta-based absorber on a low thermal expansion material (LTEM) substrate. We used two types of mask blanks fabricated by different processes: Sample A, in which the film adhesion between top-Si and Ru capping was deliberately weakened, and Sample B, which was fabricated as the commercial design. We also prepared the EUV photomask fragments based on non-AGC mask blanks. The photomask structures were the same as Fig. 3, but materials and fabrication processes were different.

3 Blister formation

3.1 Mask blanks

Table 1 shows the EUV accelerated lifetime test results for the mask blank fragments #1 to #10. Samples #1 to #4 were irradiated under hydrogen at 5, 15, 30, and 70 Pa with an EUV intensity of around 35 W/cm^2. Blisters appeared after 230, 165, and 110 minutes at 15, 30, and 70 Pa, corresponding to onset doses of 500.0, 344.4, and 229.6 kJ/cm^2, whereas no blister formed at 5 Pa within 8 hours. Samples #5 to #7 were irradiated at the same hydrogen pressures with water vapor added at a constant 10^{-3} Pa, giving EUV doses of 622.1, 213.0, and 206.5 kJ/cm^2 at 5, 30, and 70 Pa. Samples #8 and #9 extended the water vapor pressure to 10^{-2} and 10^{-1} Pa at 70 Pa of hydrogen. Sample B (#10) was irradiated for 385 minutes at 42.70 W/cm^2 under 70 Pa of hydrogen with 10^{-3} Pa of water vapor, and showed no blister up to 986.4 kJ/cm^2.

Fig. 4 shows the blister formation dependence on the hydrogen pressure. The required dose decreased as the hydrogen pressure increased with and without water vapor, and adding water vapor lowered it at every pressure. The reduction was 23.1 kJ/cm^2 at 70 Pa (#7 versus #4) and 131.4 kJ/cm^2 at 30 Pa (#6 versus #3). The effect was largest at 5 Pa, where no blister formed under hydrogen within 1004.3 kJ/cm^2 (#1) but appeared after 622.1 kJ/cm^2 once water vapor was added (#5).

Fig. 5 shows the blister formation dependence on the water vapor pressure at a fixed hydrogen pressure of 70 Pa. Raising the water vapor pressure from 10^{-3} to 10^{-1} Pa reduced the dose from 206.5 to 174.7 kJ/cm^2, a 15 % change over two decades. The introduction of water vapor itself accounted for a comparable 10 % reduction relative to hydrogen (#4, 229.6 kJ/cm^2), so the effect saturates rapidly above 10^{-3} Pa.

Fig. 6 shows the EUV dose dependence of blister formation on EUV intensity around 35 W/cm^2 and 20 W/cm^2 under hydrogen. The case of 35 W/cm^2 is referred from sample #2, #3 and #4. The two datasets agree within 7 % at every hydrogen pressure, and the difference is smaller than the pressure-induced change of the EUV dose by more than an order of magnitude. The dose can be compared between samples irradiated at different intensities in Table 1.

Table 1 Hydrogen and water vapor plasma durability test results on EUV mask blanks

No.	Sample	EUV intensity (W/cm^2)	H_2 Pressure (Pa)	H_2O Pressure (Pa)	Blister	Blister formation time (min)	Blister formation dose (kJ/cm^2)
1	Sample A	34.87	5	0	None		
2		36.23	15	0	**Observed**	230	500.0
3		34.79	30	0	**Observed**	165	344.4
4		34.79	70	0	**Observed**	110	229.6
5		35.75	5	10^{-3}	**Observed**	290	622.1
6		39.89	30	10^{-3}	**Observed**	89	213.0
7		36.22	70	10^{-3}	**Observed**	95	206.5
8		34.27	70	10^{-2}	**Observed**	92	189.2
9		30.97	70	10^{-1}	**Observed**	94	174.7
10	Sample B	42.70	70	10^{-3}	None		

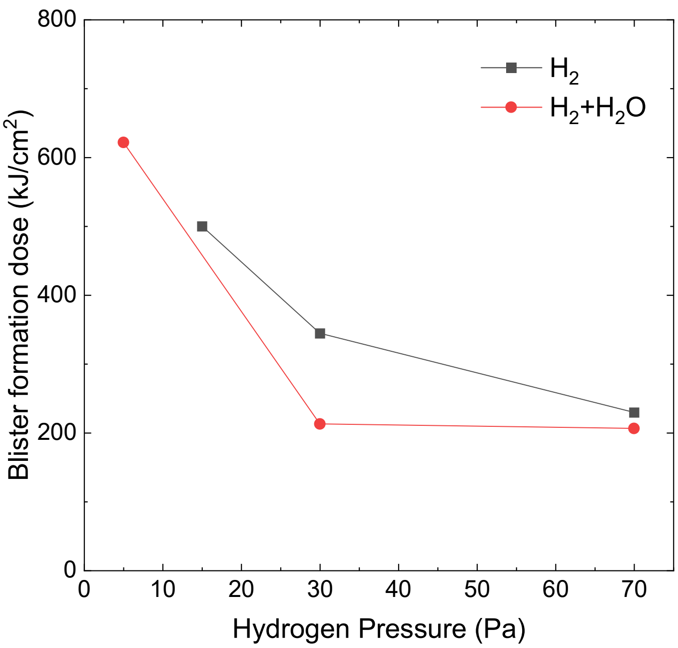

Fig. 4 EUV dose dependence of blister formation on hydrogen pressure and water vapor of 10^{-3} Pa on the mask blanks #2-7.

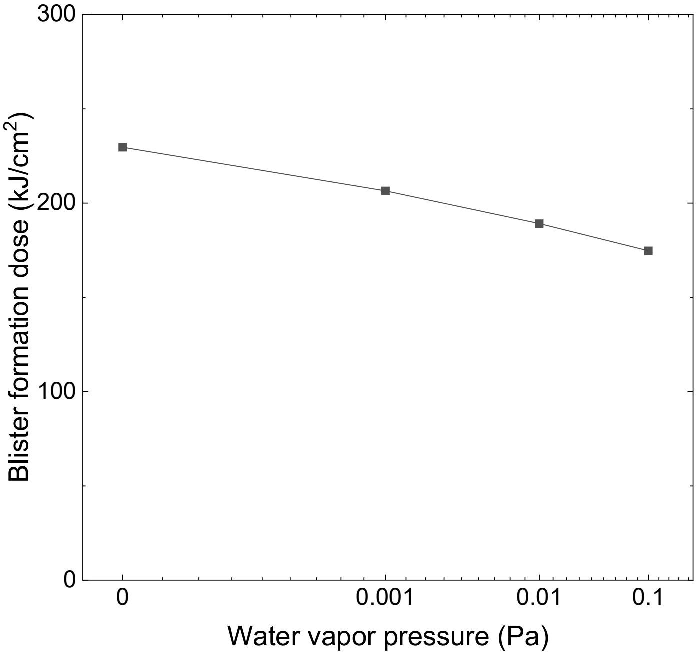

Fig. 5 EUV dose dependence of blister formation on water vapor pressure with hydrogen of 70 Pa on the mask blanks #4 and #7-9.

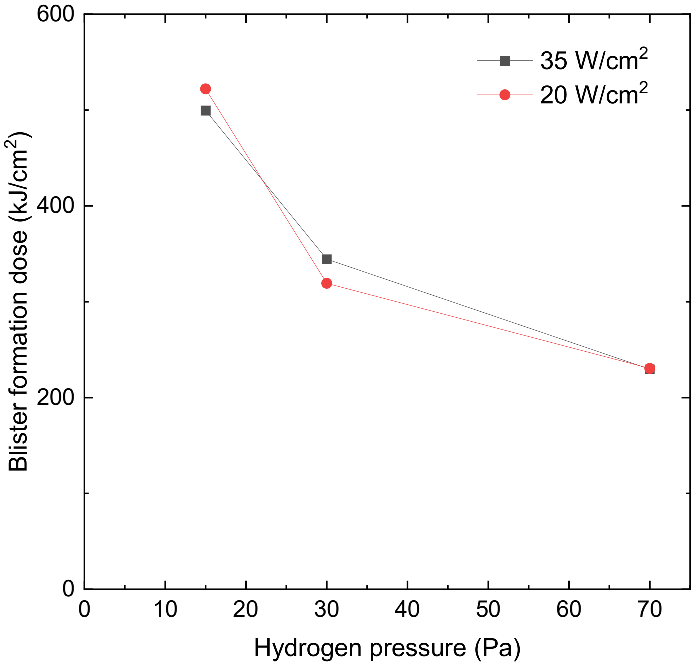

Fig. 6 EUV dose dependence of blister formation on EUV intensity between 35 W/cm^2 and 20 W/cm^2 under hydrogen.

Fig. 7 shows microscope images of the blisters and film delamination. Under hydrogen at 30 and 70 Pa (#3 and #4), circular delamination was observed at four and six locations with one blister, respectively. These diameters are about 50 µm, while at 15 Pa (#2) a single blister of approximately 100 µm was observed. With water vapor, larger blisters of about 400 µm appeared at 30 and 70 Pa (#6 and #7), and at 5 Pa (#5) delamination accompanied by film floating was observed.

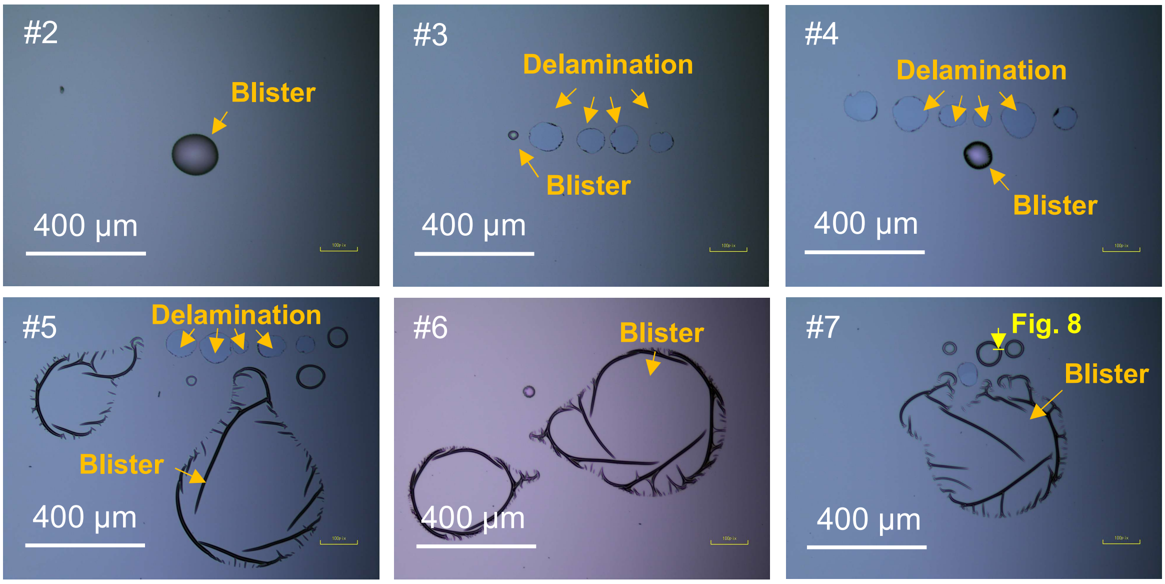

Fig. 7 Microscope images of blister formation on the mask blanks.

Fig. 8-(a) shows the scanning electron microscopy (SEM) image of the blisters on the mask blank #7 after the EUV acceleration tests with hydrogen and water vapor at the blister position. Fig. 8-(b) shows the cross-sectional scanning transmission electron microscopy (STEM) image cut along the yellow dashed line of Fig. 8-(a). C capping layer was deposited on the absorber for cutting process. A blister was observed at the interface between the Ru capping layer and the top-Si layer of the ML, and no delamination within the ML.

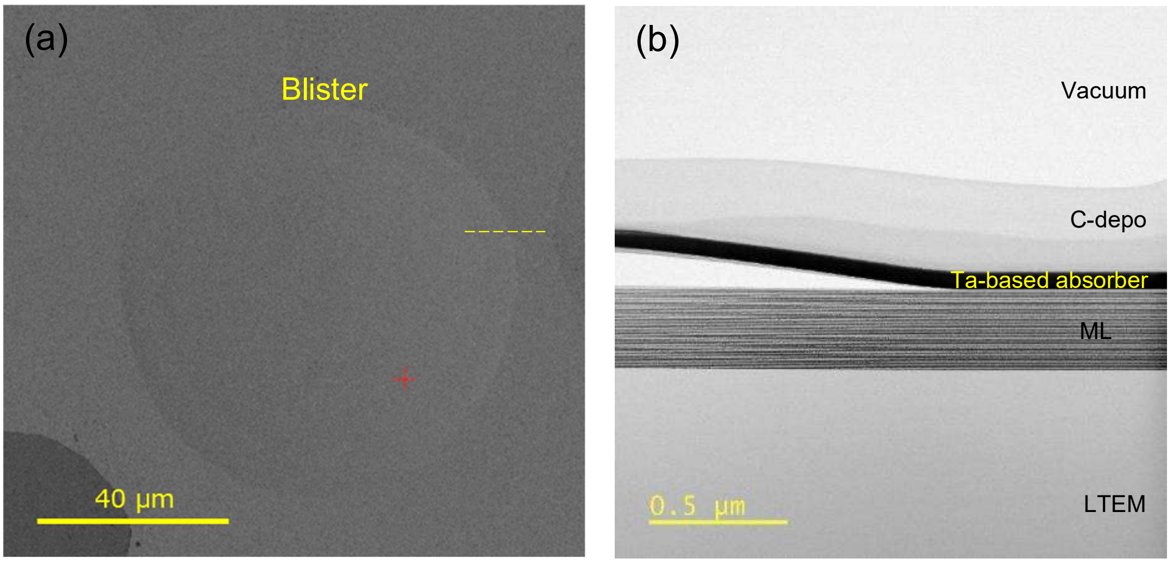

Fig. 8 (a) SEM image of blister on the surface of the mask blank #7 after the EUV irradiation with hydrogen and water vapor at the blister position, (b) Cross-sectional STEM image observed along the yellow dashed line of Fig. 8-(a).

3.2 Photomasks

Table 2 shows the EUV accelerated lifetime test results on the photomask fragments #11 and #12. The samples #11 and #12 were tested under 5 Pa of hydrogen, and additional 10^{-3} of water vapor. Blisters were observed in both samples, with EUV doses of 178.9 kJ/cm² for #11 and 108.6 kJ/cm² for #12. The introduction of water vapor reduced about 39% of the blister formation dose that reproduced the trend in Fig. 4, even the masks were designed with different materials and processes.

Table 2 Hydrogen and water vapor plasma durability test results on EUV photomasks

No.	Sample	EUV intensity (W/cm^2)	H_2 Pressure (Pa)	H_2O Pressure (Pa)	Blister	Blister formation time (min)	Blister formation dose (kJ/cm^2)
11	Photomask	47.32	5	0	**Observed**	63	178.9
12		31.74	5	10^{-3}	**Observed**	57	108.6

4 Surface analysis

4.1 XAS profile on mask blanks

We measured the EUV reflectivity of 13.5 nm wavelength to identify the irradiated and the unirradiated positions on the mask blanks #3 and #6 as shown in Fig. 9. The measurement is x-axis scanning of reflectivity through 5 mm including the irradiated region. At the irradiated positions, the increase of approximately 4 % in reflectivity was observed under hydrogen only conditions, suggesting pin-hole delamination occurred within the beam spot size. In contrast, the condition of hydrogen with water vapor, the increase of approximately 0.5 % was observed.

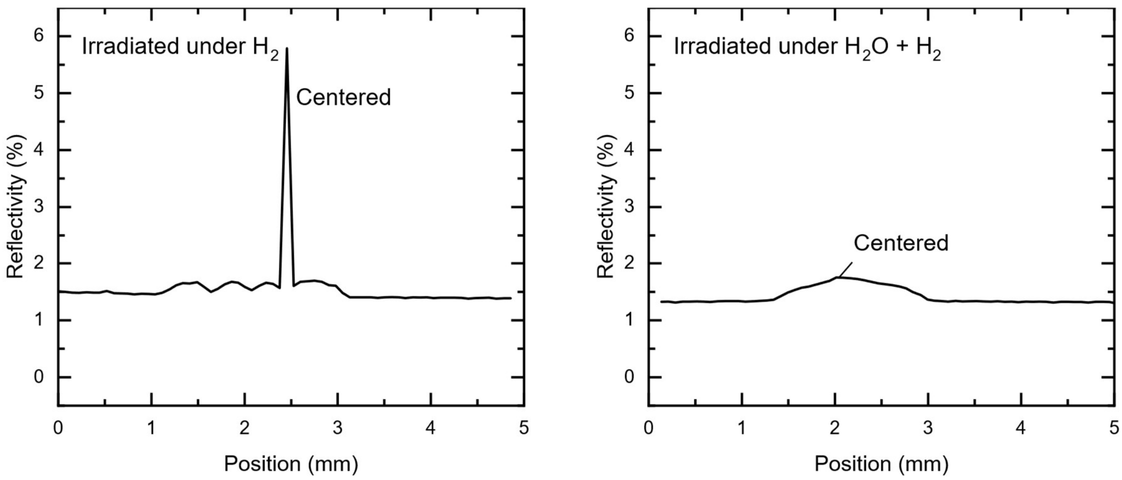

Fig. 9 EUV reflectivity of the irradiated and the unirradiated positions on the mask blanks #3 and #6.

We measured the surface oxidation using O *K*-edge energy from X-ray absorption spectroscopy (XAS) on #3 and #6. Fig. 10 shows the total electron yield (TEY)-mode XAS spectra measured in vacuum state, to compare the oxidation between the unirradiated and irradiated positions on surface of the mask blanks #3 and #6. The results show significant differences in the intensity around 543 eV, indicating that oxidation occurred in both the hydrogen-only and the water vapor cases. It suggests that the oxidation was not only induced by water vapor, but oxide materials arising from oxidation of Ta-base absorber and top-Si oxide of Mo/Si ML interacted with hydrogen to boost oxidation.

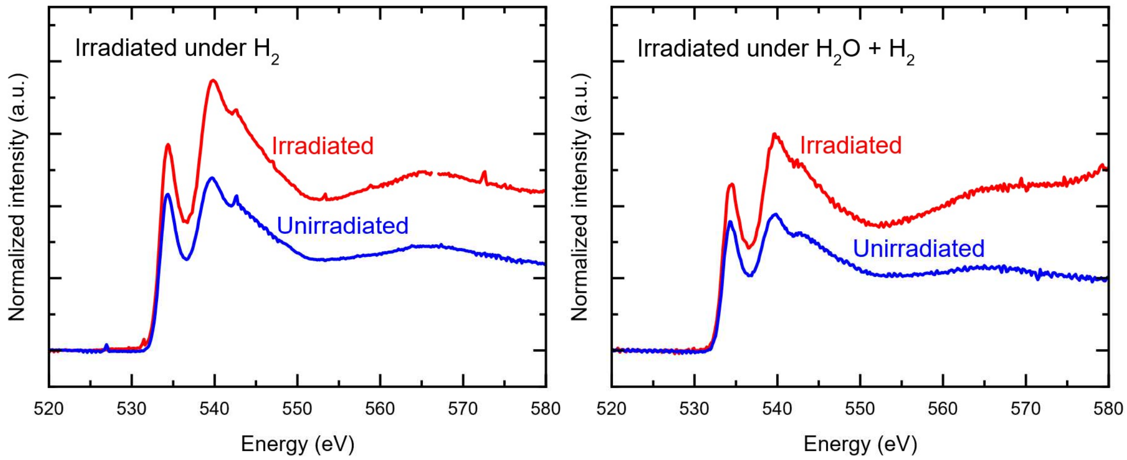

Fig. 10 XAS spectra on the mask blanks #3 and #6 after the EUV irradiation at the blister positions.

4.2 Hydrogen profile on photomasks

We measured the hydrogen content by Rutherford backscattering spectrometry (RBS) and hydrogen forward scattering spectrometry (HFS) using a 2300 keV $^{4}He^{2+}$ beam with a 0.5 mm spot. The incident angle was 75° from the surface normal and recoiled hydrogen was detected at 30° through a range foil that rejected forward scattered He ions. RBS spectra were recorded simultaneously at 160° for elemental composition and charge normalization, and absolute hydrogen concentrations were obtained by reference to a standard of known hydrogen content.

Fig. 11 shows the RBS results for the nanoscale-converted elemental depth profiles of the photomask #12 in the unirradiated (5 mm apart from the center) and the irradiated positions. In the unirradiated and irradiated profiles, hydrogen was concentrated near the surface at depths of around 0 to 15 nm, accompanied by carbon and minor amounts of oxygen and nitrogen. After irradiation, hydrogen was detected at an approximately constant atomic ratio of 0.02 through the Ta-based absorber and the Ru capping layer, where the unirradiated profile showed none below 15 nm, and the excess extended about 30 nm into the Mo/Si ML, before falling below 0.001 at 97 nm. The Mo and Si ratios in the ML were unchanged between the two positions, indicating that the multilayer structure itself was not modified by the irradiation.

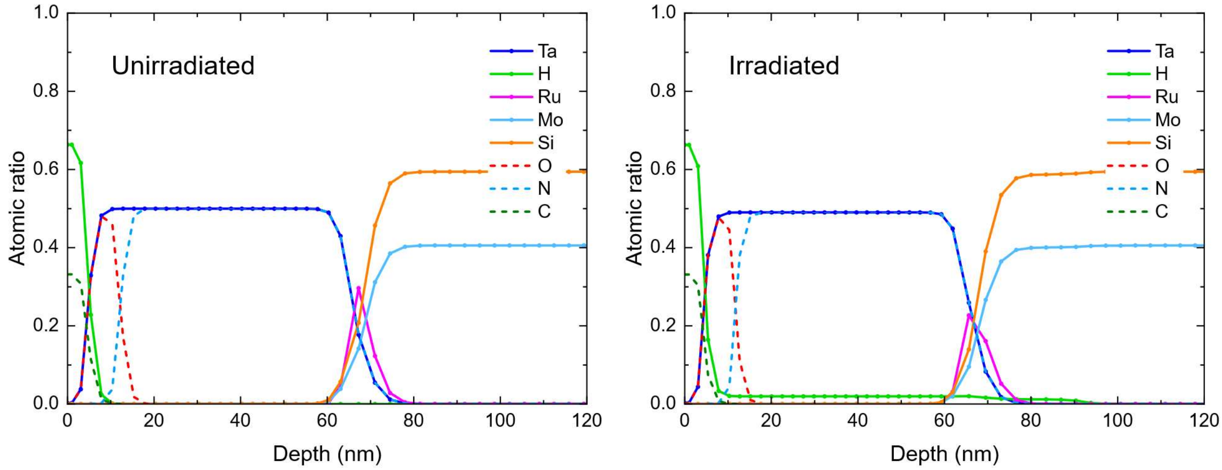

Fig. 11 RBS results of the photomask #12 in the unirradiated and the irradiated positions.

Fig. 12 shows the HFS spectra obtained from the unirradiated and irradiated regions of photomask #12. The beam conditions were the same as in the RBS measurement, and recoiled hydrogen was detected at a forward angle of 30°. In HFS, hydrogen atoms located at greater depths are detected at lower energies owing to the larger energy loss during scattering. The result indicates that hydrogen near the surface gave rise to the main peak at around 750-800 keV, whereas hydrogen distributed deeper in the structure appeared on the lower-energy side of the spectrum. The irradiated region showed a higher hydrogen yield than the unirradiated region in the 600-740 keV range.

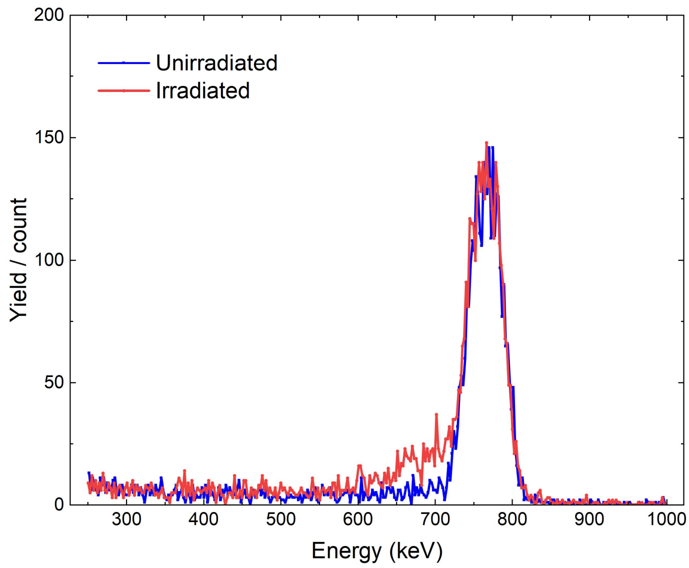

Fig. 12 HFS results of the photomask #12 in the unirradiated and the irradiated regions.

5 Discussion

The threshold EUV dose for blister formation decreases with hydrogen pressure, following approximately an inverse square-root dependence between 15 and 70 Pa. Assuming that blisters were governed by the photon dose alone, no such dependence would appear and the hydrogen supply to the interface is rate-limiting, and blistering is initiated once a critical hydrogen concentration has accumulated, confirmed by the RBS results. The hydrogen signals increased down to the Mo/Si ML while the Ta, Si and Mo ratios were unchanged. This depth is consistent with the Ru/top-Si delamination seen by STEM, with no delamination inside the ML.

XAS shows oxidation both with and without water vapor, so oxygen released from the native oxide on the Ta-based absorber and top-Si of Mo/Si is already mobilized by the plasma, and water vapor is an additional rather than the exclusive source. At 10^{-3} Pa its pressure is four to five orders of magnitude below that of hydrogen, so that the effect is expected to proceed through water vapor dissociated by secondary electrons. Furthermore, raising the water vapor pressure by two decades to 10^{-1} Pa gave only a 15 % further reduction, indicating that the oxygen originating from the mask itself also boosts blister formation.

The impact of water vapor grows as the hydrogen pressure falls, from 10 % at 70 Pa to blistering at 5 Pa where hydrogen produced none. Since water vapor cannot increase the hydrogen flux, it is expected to act on the opposite side of the balance by oxidizing the interface between Ru and top-Si of ML, lowering its adhesion energy. Sample B, of commercial design, withstood 986.4 kJ/cm² whereas the deliberately weakened Sample A blistered at 206.5 kJ/cm², identifying that film adhesion control such as oxidation of interfacial layers is the one of target for mask process development.

6 Conclusion

We investigated blister formation on EUV mask blanks and photomasks under EUV-induced plasma environments with hydrogen and water vapor through EUV accelerated lifetime tests. The EUV dose decreased from 500.0 to 229.6 kJ/cm² as the hydrogen pressure increased from 15 to 70 Pa, and no blister appeared at 5 Pa within 8 hours. Adding water vapor at 10^{-3} Pa lowered the onset dose at every hydrogen pressure, triggered blistering even at 5 Pa, and reduced the dose by approximately 39 % on the photomask. A further increase to 10^{-1} Pa gave a 15 % additional reduction, indicating the blister formation dependence on the water vapor pressure. The delamination occurred at the interface between the Ru capping layer and the top-Si of ML, accompanied by surface oxidation and hydrogen accumulation from the absorber into the ML. These threshold values quantify mask lifetime and provide a basis for mask blank design and process control.

Disclosures

The authors declare that there are no financial interests, commercial affiliations, or other potential conflicts of interest that could have influenced the objectivity of this research or the writing of this paper.

Code, Data, and Materials Availability

The data that supports the findings of this study are available from the corresponding authors on request.

Acknowledgments

This work was partially supported by Hyogo Earthquake Memorial 21st Century Research Institute, Hyogo Foundation for Science and Technology, Tanaka Kikinzoku Memorial Foundation, Takahashi Industrial and Economic Research Foundation, and Foundation of Kinoshita Memorial Enterprise.

References

1. J. van Schoot, “Exposure tool development toward advanced EUV lithography: A journey of 40 years driving Moore’s law,” *IEEE Electron Devices Magazine* **2**(1), 8-22 (2024)
2. A. Barty and K. A. Goldberg, "Effects of radiation-induced carbon contamination on the performance of an EUV lithographic optic," *Proc. SPIE* **5037** 450-459 (2003).
3. Y. Nishiyama et al., "Carbon contamination of EUV mask: film characterization, impact on lithographic performance, and cleaning," *Proc. SPIE* **6921**, 338-347 (2008).
4. N. B. Koster et al., "A multistep approach for reticle cleaning," *Proc. SPIE* **8322** 217-227 (2012).
5. A. Dolgov et al., "Comparison of H2 and He carbon cleaning mechanisms in extreme ultraviolet induced and surface wave discharge plasmas," *J. Phys. D: Appl. Phys.* **47**(6), 065205 (2013).

6. J. M. Pommersheim et al., "Prediction of blistering in coating systems," *Organic Coatings for Corrosion Control*, Chap. 11, 137-150 (1998).
7. A. S. Kuznetsov et al., "Blistering behavior in Mo/Si multilayers," *Proc. SPIE* **8077**, 253-260. (2011).
8. T. Hiroaki et al., "Evaluation of hydrogen-induced blistering of Mo/Si multilayers with a capping layer," *Plasma Fusion Res.* **17**, 1406005 (2022).
9. E. S. Choe et al., "Evaluation of H2 Plasma‐Induced Damage in Materials for EUV Lithography," *Adv. Mater. Interfaces* **11**(7), 2300867 (2024).
10. H. Ishida et al., “Development of an EUV irradiation tool in hydrogen atmosphere to evaluate EUV mask absorber durability,” *Jpn. J. Appl. Phys.* **64**(3), 03SP71 (2025).
11. R. Klein et al., "Lifetime testing of EUV optics using intense synchrotron radiation at the PTB radiometry laboratory," *Proc. SPIE* **4506**, 105-112 (2001).
12. C. C. Wu et al., “Lifetime test on EUV photomask with EBL2,” *Proc. SPIE* **11178**, 94-99 (2019).
13. T. Harada et al., "Development of a high-power EUV irradiation tool in a hydrogen atmosphere," Jpn. *J. Appl. Phys.* **60**(8), 087005 (2021).
14. J. K. Stortelder et al., “First experimental evaluation of accelerated reticle lifetime testing using an applied bias voltage at EBL2,” *Proc. SPIE* **13687**, 75-84 (2025).
15. R. Jonckheere et al., "Study of EUV reticle storage effects through exposure on EBL2 and NXE," *Proc. SPIE* **11517**, 78-90 (2020).
16. G. Yetik et al., "Real-time observation of EUV-induced blister formation at various sample temperatures in pellicle-like materials," *Proc. SPIE* **13686**, 206-218 (2025).
17. J. Stortelder et al., "Compatibility assessment of novel reticle absorber materials for use in EUV lithography systems," *Proc. SPIE* **10957**, 259-267 (2019).
18. J. Stortelder et al., "First results of EUV-scanner compatibility tests performed on novel 'high-NA' reticle absorber materials," *Proc. SPIE* **11854**, 103-114 (2021).
19. M. van de Kerkhof et al., "Plasma-assisted discharges and charging in EUV-induced plasma," *J. Micro/Nanopattern. Mater. Metrol.* **20**(1), 013801 (2021).
20. M. van de Kerkhof et al., "EUV-induced hydrogen plasma: pulsed mode operation and confinement in scanner,” J. Micro/Nanopattern. Mater. Metrol. **20**(3), 033801 (2021).
21. M. van de Kerkhof et al., "EUV-induced hydrogen plasma and particle release," *Radiat. Eff. Defects Solids* **177**(5-6), 486-512 (2022).
22. K.W. Lu et al., “The effect of hydrogen ion bombardment on the capping layers of extreme ultraviolet mirrors,” *Mater. Res. Express* **12**(4), 046402 (2025).
23. N. Koster, B. Mertens, R. Jansen, A. Van De Runstraat, F. Stietz, M. Wedowski, H. Meiling, R. Klein, A. Gottwald, F. Scholze, M. Visser, R. Kurt, P. Zalm, E. Louis, A. Yakshin, “Molecular

contamination mitigation in EUVL by environmental control," *Microelectron. Eng.* **61-62**, 65-76 (2002).

24. T. E. Madey et al., "Surface phenomena related to mirror degradation in extreme ultraviolet (EUV) lithography," *Appl. Surf. Sci.* **253**(4) 1691-1708 (2006).
25. A. L. Bondareva, G. I. Zmievskaya, "Computer simulation of blistering in multilayer mirrors for EUV lithography," *J. Surf. Investig.: X-ray Synchrotron Neutron Tech.* **4**(3) 480-487 (2010).
26. T. H. M. Van De Ven et al., "Ion energy distributions in highly transient EUV induced plasma in hydrogen," *J. Appl. Phys.* **123**(6) (2018).
27. L. P. Ramírez, F. Bournel, J. J. Gallet, L. Dudy, F. Rochet, "Testing the Cabrera–Mott oxidation model for aluminum under realistic conditions with near-ambient pressure photoemission," *J. Phys. Chem. C* **126**(5), 2517-2530 (2022).
28. J. D. Baran, H. Grönbeck, A. Hellman, "Mechanism for limiting thickness of thin oxide films on aluminum," *Phys. Rev. Lett.* **112**(14), 146103 (2014).
29. M. van de Kerkhof, "Interaction between EUV and construction materials," *Proc. SPIE* **13533**, 37-41 (2025).
30. N. Cabrera, N. F. Mott, "Theory of the oxidation of metals," *Rep. Prog. Phys.* **12**(1) 163 (1949).
31. E. A. Gulbransen et al., "Oxidation of Molybdenum 550 to 1700 C," *J. Electrochem. Soc.* **110**(9), 952 (1963).
32. M. R. Louthan Jr et al., "Hydrogen embrittlement of metals," *Mater. Sci. Eng.* **10**, 357-368 (1972).
33. M. van de Kerkhof et al., "High-transmission EUV pellicles supporting > 400W source power," *Proc. SPIE* **12051**, 70-77 (2022).

Biographies and photographs for the other authors are not available.